AGU100 ADVANCING EARTH AND SPACE SCIENCE

Radio Science

RESEARCH ARTICLE
10.1029/2017RS006428

Key Points:
- Neutral wind and electric field influence EIA asymmetries
- An electric field at the equator can alone form the symmetric structure of EIAs
- Meridional neutral wind is a decisive factor of the asymmetry structure of EIAs

Correspondence to:
S. M. Khadka,
khadkas@bc.edu

Citation:
Khadka, S. M., Valladares, C. E., Sheehan, R., & Gerrard, A. J. (2018). Effects of electric field and neutral wind on the asymmetry of equatorial ionization anomaly. *Radio Science*, *53*, 683–697. https://doi.org/10.1029/2017RS006428

Received 25 AUG 2017
Accepted 3 APR 2018
Accepted article online 17 APR 2018
Published online 26 MAY 2018

Effects of Electric Field and Neutral Wind on the Asymmetry of Equatorial Ionization Anomaly

Sovit M. Khadka[1,2], Cesar E. Valladares[3], Robert Sheehan[2], and Andrew J. Gerrard[4]

[1]Physics Department, Boston College, Chestnut Hill, MA, USA, [2]Institute for Scientific Research, Boston College, Newton, MA, USA, [3]W. B. Hanson Center for Space Sciences, University of Texas at Dallas, Richardson, TX, USA, [4]Center for Solar-Terrestrial Research, New Jersey Institute of Technology, Newark, NJ, USA

Abstract The zonal electric field and the meridional neutral wind are the principal drivers that define the geometry and characteristics of the equatorial ionization anomaly (EIA). Here we present the response of the EIA to the variability of the zonal electric field based on measurements of the equatorial electrojet (EEJ) currents and trans-equatorial neutral winds for the generation and control of the asymmetries of the EIA crests of total electron content (TEC) in the western side of the South American continent. The EEJ strengths are determined using a pair of magnetometers. The 24-hr trans-equatorial neutral wind profile is measured using the Second-Generation, Optimized, Fabry-Perot Doppler Imager (SOFDI) located near the geomagnetic equator. The EIA is evaluated using TEC data measured by Global Positioning System (GPS) receivers from the Low-Latitude Ionospheric Sensor Network and several other networks in South America. A physics-based numerical model, Low-Latitude Ionospheric Sector, and SOFDI data are used to study the effects of daytime meridional neutral winds on the consequent evolution of an asymmetry in equatorial TEC anomalies during the afternoon and onward for the first time. We find that the configuration parameters such as strength, shape, amplitude, and latitudinal width of the EIAs are affected by the eastward electric field associated with the EEJ under undisturbed conditions. The asymmetries of EIA crests are observed more frequently during solstices and the September equinox than in the March equinox season. Importantly, this study indicates that the meridional neutral wind plays a very significant role in the development of the EIA asymmetry by transporting the plasma up the field lines. This result suggests that a precise observation of the latitudinal TEC profile at low latitudes can be used to derive the meridional wind.

1. Introduction

The equatorial ionosphere is a popular area of research for the space weather community due to its unique structuring, coupling, and electrodynamics. The ionosphere exhibits both slow and rapid responses to changes in its fundamental input mechanisms, including variation induced by electric fields, plasma-neutral coupling, and modulation by solar and geomagnetic disturbances. Several observable quantities of the daytime equatorial and low-latitude ionospheric phenomena offer the possibility to forecast the dynamics and fluctuations of ionospheric plasma densities at later times. For example, the ionospheric electric fields, plasma drifts, and currents generally result from the dynamo action of *E* and *F* region neutral winds driven by solar and lunar tides in the low and middle latitudes. The ionospheric electric field is produced by the motion of plasma maintaining its fundamental properties, such as its collective behavior and the state of quasi-neutrality. Furthermore, polarization fields, conductivity variations, and atmospheric gravity and planetary waves can also significantly affect timescales from tens of minutes to about a month (Eccles et al., 2011; Fejer, 1991; Kelley, 2009; Richmond, 1989).

The equatorial electrojet (EEJ) and equatorial ionization anomaly (EIA) are prominent daytime effects of the low-latitude ionospheric phenomena that are driven by the eastward electric field (EEF) (Heelis, 2004; MacDougall, 1969). The EEJ (Chapman, 1951) is one of the unique daytime ionospheric phenomena, defined as an intense eastward current flowing in the form of a ribbon-shaped band roughly 600 km wide in the *E* region ionosphere flanking the geomagnetic equator of the Earth (Egedal, 1947; Forbes, 1981; Onwumechili, 1997). The pressure gradients from solar and auroral heating, with additional forcing by tidal energy from below, are possible drivers of the thermospheric neutral winds (Blanc & Richmond, 1980; Titheridge, 1995). During magnetically quiet periods, the atmospheric wind dynamo mechanism within ±60° geomagnetic latitudes is the main driver of the ionospheric electric fields and currents in which ions and electrons move under the control of neutral winds and electric and magnetic fields (Richmond, 1989;

Rishbeth, 1997). The atmospheric wind at ionospheric heights sets a tidal motion current due to differential solar heating in the Northern and Southern Hemisphere that converges at the geomagnetic equator and forms a jet-like current in the ionosphere. In addition, the special geometry of the geomagnetic field at the equator, together with the nearly perpendicular incidence of solar radiation, causes an equatorial enhancement in the effective conductivity, which then leads to an amplification of the jet current that forms a belt-like structure flowing eastward during the day along the geomagnetic equator in the *E* region ionosphere (Baumjohann & Treumann, 2012; Onwumechili, 1997), forming the EEJ. This enhanced EEF acts perpendicular to the northward geomagnetic field at equatorial latitudes and lifts up plasma with vertical $\mathbf{E} \times \mathbf{B}$ drift to higher altitudes. When plasma is elevated to higher altitudes, it diffuses downward along the geomagnetic field lines due to gravitational and pressure gradient forces to about ±17° latitudes on both sides of the geomagnetic equator. This mechanism is known as the equatorial plasma fountain effect (Anderson, 1973; Appleton, 1946; Martyn, 1947; Schunk & Nagy, 2000). The fountain effect removes plasma from the equator and creates a pair of electron density crests at about ±17° either sides of the geomagnetic equator, forming the EIA. The EIA was discovered by Edward V. Appleton (1946) and is also known as the Appleton anomaly. Indeed, an equatorial EEF is a vital ingredient in generating EIAs and a key participant in the onset of equatorial plasma bubbles. EIA onset is identified by an EEF that subsequently expands to symmetrically $<20°$ latitudes either sides of the equator. Nevertheless, the strength of the EIA crest in one hemisphere is commonly stronger than that of the opposite hemisphere forming an asymmetry structure. A long-standing research question in thermosphere-ionosphere coupling system is the process responsible for the asymmetry generation on the EIA. However, the EEJ cannot alone give sufficient evidence of asymmetry structure of the EIAs, and the ultimate aim of the present paper is to report the results obtained from a study of the electric field as well as neutral wind dependence of the EIA structure.

The thermospheric wind also plays a significant role by controlling the vertical positions of the *F* region pushing ions along the magnetic field lines and contributes to the unequal magnitude of EIA crests as well as the formation of additional ionospheric layers (Herrero et al., 1993; Lin et al., 2009; Makela et al., 2013; Rishbeth, 1972). Neutral winds cause interhemispheric asymmetry in EIAs by modulating the plasma fountain and moving the ionospheres at the conjugate hemispheres to different altitudes (Balan et al., 1995; Dang et al., 2016). The seasonal, solar activity, temporal, and longitudinal variations in EIA asymmetry also depend on the displacement of the geographic and geomagnetic equators and in the magnetic declination angle (Dang et al., 2016; Luan et al., 2015; Su et al., 1997; Tulasi Ram et al., 2009), which is the largest in the American sector. The change in magnitude and direction of the neutral wind field initiated by global or local pressure distribution and ambipolar diffusion associated with neutral density and scale height is one of the prime candidates to govern the variability of EIA (Kelley, 2009; Sastri, 1990). The ions and neutral particles are dynamically coupled with each other through ion-neutral collisions via meridional neutral wind, which is responsible for the asymmetric generation of the EIAs by controlling the final location of the enhanced total electron content (TEC) in the equatorial ionosphere (Hei & Valladares, 2010; Valladares & Chau, 2012). In contrast to the large number of studies on thermospheric neutral winds and EIA, heretofore, daytime measured meridional neutral winds and their role in structural dynamics of EIAs have not been fully addressed. The ground-based Fabry-Perot interferometer has shown significant effectiveness in the measurement of thermospheric neutral winds, but it is restricted to cloudless nighttime observations only (Burnside et al., 1981; Hedin et al., 1991; Makela et al., 2012; Meriwether, 2006). There are various limitations to obtain flawless daytime measured thermospheric neutral winds in the upper atmosphere. While there has been intense debate on the capability of various methods and models for the estimation of daytime meridional neutral winds, Gerrard and Meriwether (2011) developed a new design of triple-etalon interferometer, called Second-generation, Optimized, Fabry-Perot Doppler Imager (SODFI), that is able to make 24-hr measurements of thermospheric winds from OI 630-nm emission in the geomagnetic equatorial regions.

Our understanding of the role played by ionospheric electric fields and neutral winds in the formation of EIAs is still very limited despite studies done over several decades. In this study, the structural pattern of EIA strengths is observed using several networks of Global Positioning System (GPS) receivers, while the trans-equatorial neutral winds are determined using the Second-generation, Optimized, Fabry-Perot Doppler Imager (SOFDI). Both are operated in the equatorial and low-latitude regions of South America. The Jicamarca incoherent scatter radar (ISR) allows for real-time equatorial vertical plasma drifts. Simultaneously, the physics-based Low-Latitude IONospheric Sector (LLIONS) model is also used to

estimate daytime meridional neutral winds by taking the Jicamarca ISR vertical drifts as one of the model's inputs. A meridional neutral wind was inferred using the LLIONS model due to the fact that there are not enough measured wind values during the daytime. Such model-inferred meridional wind results are compared with measured values provided by the SOFDI located in Huancayo, Peru. We found a significant correlation of the symmetry and asymmetry of EIA anomaly patterns with EEJ and meridional neutral wind respectively during quiet conditions. Thus, these observational and modeling efforts suggest that the meridional neutral wind influences the generation of asymmetry of EIAs in the Earth's low-latitude ionosphere. A full understanding of the link between the neutral winds and asymmetry structures of EIAs in the ionosphere requires higher resolution wind measurements. Finally, a mechanism describing the physics behind the plasma flow for the generation of asymmetry on EIAs is presented.

2. Instrumentation, Data sets, and Methodology

The low-latitude region of the western meridian in the South American continent is well instrumented with magnetometers, GPS receivers, Fabry-Perot interferometers, radars, and different types of ionosondes. We present dual-frequency GPS TEC data sets to study the strength, occurrence, and latitudinal distribution of EIAs around the 75°W longitude in the equatorial and low-latitude ionosphere. The Low-Latitude Ionospheric Sensor Network (LISN) is a distributed observatory that operates in the South American continent. It was designed to probe the disturbed and undisturbed ionospheric electrodynamics in the low latitudes and also allows us to explore the development as well as the decay of the EIA in unprecedented detail. GPS receivers can continuously measure TEC integrated along the line-of-sight from GPS satellites to receiver. TEC is measured in units of TECU (1 TEC Unit = 10^{16} electrons/m^2).

The EEJ strength is a widely accepted proxy for the daytime EEF in the ionospheric E-region (Deshpande et al., 1977; Dunford, 1967; Stolle et al., 2008). The EEJ is estimated using the variability of the horizontal components of Earth's magnetic field intensity (denoted *H*) data from a pair of ground-based magnetometers. The strengths of the *H* component data are recorded using fluxgate magnetometers at a geomagnetic equatorial station, Jicamarca (geog. 11.9°S, 283.1°E, 0.8°N dip latitude) and an off-equatorial station, Piura (geog. 5.2°S, 279.4°E, 6.8°N dip latitude) in the American low latitudes. As described in Khadka et al. (2016), magnetometer readings of H from each station are normalized with its midnight average background values for each day and subtracted to get only the electrojet contribution to H. The difference of electrojet effect on *H* between two magnetometers located at equator and off-equator (6° to 9° away) is defined as the EEJ strength.

The meridional neutral wind is measured using a specially designed interferometer system, SOFDI, and a physics-based numerical model data. SODFI is a unique ground-based instrument and has a broad range of applications pertaining to both daytime and nighttime observations of the mesosphere and thermosphere airglow emissions. We use meridional neutral wind data collected during daytime using SOFDI at the equatorial station Huancayo (geog. 12.7°S, 284.8°E, and 0.6° S dip latitude), Peru. The detailed optical geometry, instrumentation, observation, and extraction of neutral wind data by removing the background from dayglow emission is explained in Gerrard and Meriwether (2011).

For the present study, the day to day variability of TEC for the years 2011–2013 is shown to introduce the asymmetric patterns of EIA. It is found that all instruments, magnetometers, Jicamarca ISR, GPS receivers, and SOFDI operated simultaneously for a few days in August 2011; thus, we discuss in detail the observations and simulations for those days. A comparison analysis between meridional neutral wind estimated from LLIONS model and that from observed SODFI data and their contributions to EIA asymmetries is also computed.

3. Analysis and Results

The asymmetry of the EIA is investigated using equivalent vertical TEC derived from GPS receivers spread in South America. Even though the detailed information of anomaly drivers is still in debate, our analyses logically address such questions with direct measurement and modeling technique. Most of the days, the crests of TEC anomalies have an unequal strength and are separated from the magnetic equator by less than 20°. The trough of the equatorial anomaly is located at the magnetic equator. The strength of EIA asymmetry is calculated by taking the ratio of the maximum value of the two hemispheric anomaly TEC crests values. Besides the meridional neutral winds, dragging force due to continuous ion accumulation, sudden stratospheric warming, solar fluxes, atmospheric tides, change in composition due to magnetic perturbations,

and photochemical process are also responsible factors for the asymmetry of the EIA peaks (Abdu et al., 1990, 2008; Dang et al., 2016; Goncharenko et al., 2010; Hanson & Moffett, 1966; Immel et al., 2006; Jonah et al., 2015; Khadka et al., 2016; Tulasi Ram et al., 2009; Xiong et al., 2013). In this study, we particularly focused on analyzing the contribution of meridional neutral wind for the asymmetry generation of EIA using observational and modeled winds in the low-latitude ionosphere.

3.1. Annual, Seasonal and Day to Day Variability of EIA

The day-to-day variability of 3 years (2011, 2012, and 2013) of equivalent vertical TEC derived from LISN GPS receivers within 70°W–80°W longitude sector during 19:00 UT–22:00 UT are presented in Figure 1. This Figure displays the TEC variation as a function of geomagnetic latitude and month of the year. It is observed from Figure 1 that the TEC displays higher values during equinoctial months and lower values during solstice months. Most of the anomaly crests are located near ±17° magnetic latitudes during all seasons. If we focus on the TEC strength in the pair of anomaly crests, asymmetry can clearly be seen in the magnitude of the strengths. The anomaly crests are well formed and extended into the Northern Hemisphere on and around June solstice and then into the Southern Hemisphere during December solstice. This characteristic follows the fact that the Southern (Northern) Hemisphere is in summer season during December (June) solstice. A clear trend of increased ion density in the summer hemisphere compared with that in winter hemisphere is evident in all 3-year TEC profiles. Figure 1 presents clear evidence of equinoctial and solstitial asymmetry in TEC distributions. Anomaly crests are more symmetric during March equinox period than that in September equinox period. It is also seen from Figure 1 that the asymmetry events are more prominent during solstice seasons than in equinox seasons. Solar activity rises and falls with an 11-year cycle that affects ionospheric plasma dynamics as well as the intensity of geomagnetic activity. Figure 1 represents the ionospheric TEC data during the ramp up phase to solar maxima of solar cycle 24. Also, one can evidently see that the magnitude of TEC is seen increasing from 2011 toward 2013.

Figure 2 shows a 15-day mass plot of seasonal characteristics of EIA during different seasons represented by ±7 days for March and September equinox days and June and December solstice days corresponding to the years 2011 to 2013. The TEC data are chosen within 70°W–80°W longitude of low-latitude sectors during 19:00–22:00 UT (which is around 14:00–17:00 LT) period. It has been already reported that significant effects of peak (noontime) values of electric field on the EIA structural patterns can be seen within 3 hr of peak EEJ. TEC data corresponding only to geomagnetically quiet conditions is plotted to exclude effects due to prompt penetration electric fields and disturbance dynamo. The level of disturbances in the Earth's magnetic field is usually indicated using K_p index that is used to characterize the magnitude of geomagnetic storms. On the 15-day duration in each season, we choose only the days having the hourly averaged $K_p \leq 4$ as provided by http://omniweb.gsfc.nasa.gov/form/dx1.html. The six plots in the first column show the anomaly profiles in the equinox (March and September) seasons, while plots in the second column represent those of the solstice (June and December) seasons in 2011, 2012, and 2013, respectively. To determine the seasonal patterns of EIA, we construct a 15-day running average filter using a regression analysis with weighted linear least squares coefficients. The thick red curve in each plot represents the average of the corresponding scatter data distribution in that particular season. It is to be noted that out of 15 days, disturbed ($K_P > 4$) days, if existing, are excluded in the analyzed seasons. The scatterplots are interrupted for a few days due to the suppression of electrojet and hence drift by storm-induced electric fields. Figure 2 represents an overall quiet geomagnetic condition with occasional minor magnetic perturbations. During solstice, the EIA crests are found weaker and more asymmetric than during equinoxes.

Prominent features of these plots are the dominance of the northern crest that persists during all seasons. The peak of the northern crest is generally centered near 16–18° geomagnetic latitude, although during the June solstice, the northern crest seems located between 20° and 22° magnetic latitudes. However, during this season, the whole anomaly pattern seems shifted northward with a trough displaced from the magnetic equator by as much as 3°–5°. This effect is produced during the summer in the Northern Hemisphere and the large offset between the geographic and magnetic equators (12° at 75 W longitude). More symmetric anomaly events are seen in March equinox than during the September equinox. TEC values during the December solstice show higher TEC value than during the June solstice. In addition, the northern anomaly crests shift slightly toward the equator from the north with stronger southern crests than that in June solstice. This phenomenon is reasonable since there is summer in the Southern Hemisphere during December solstice season. Also, asymmetries

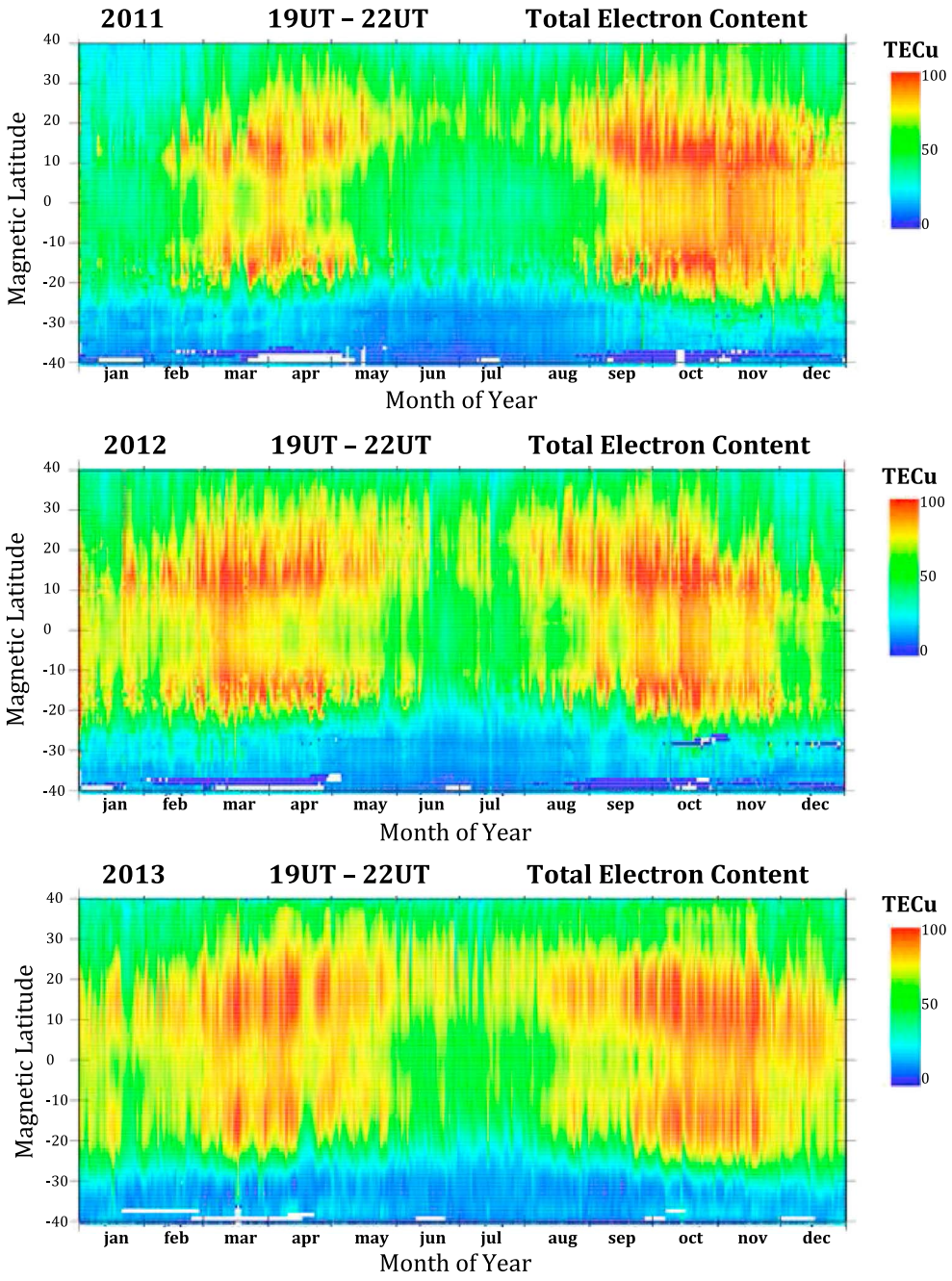

Figure 1. Geomagnetic latitudinal profiles of the annual and day-to-day variability of equatorial ionization anomaly crest of total electron content (TEC) showing an increase of the solar cycle from 2011 to 2013. The seasonal effects that alter the patterns of meridional neutral wind cause the differences of asymmetries between solstices and equinoxes.

between the hemispheric geomagnetic fields give rise to an asymmetry in the solar radiation as well as the plasma and neutral composition that ultimately leads to hemispheric differences of the electron density in the *F* region ionosphere (Laundal et al., 2016; Sojka et al., 1979). All the average curves of Figure 2 indicate that the overall strength of EIA crests in the Northern Hemisphere is stronger than the Southern Hemisphere. A reason behind this is due to the large difference of geomagnetic and geographic equator since the presented data pertain to this location. It is to be noted that western part of South America possesses the largest difference (~12°) between geomagnetic and geographic equator than any other part of the world. Moreover, the role of EEJ strength for the development of anomaly crests can be seen in a simultaneous demonstration of their measured values. Following sections attempt to address and present corresponding phenomena.

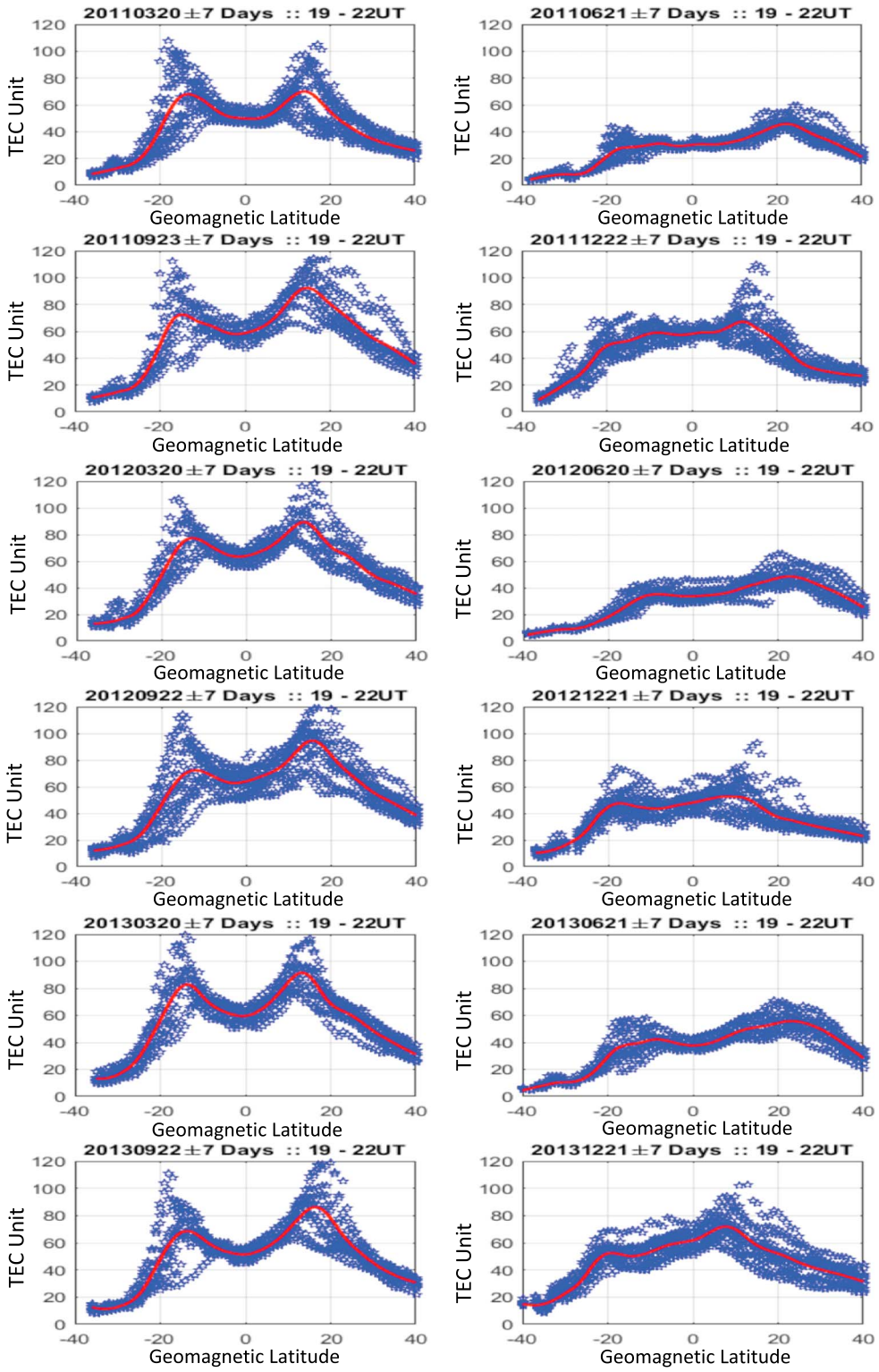

Figure 2. Fifteen-day scatterplots of latitudinal variations of maximum total electron content (TEC) data in the equinox (first column) and solstice (second column). The red continuous curve represents 15-day average of available maximum TEC.

3.2. Day-to-Day Variability of EEJ, Drifts, and EIA Strengths

The EEF associated with EEJ is a primary driving force for the vertical plasma drift. Figure 3 shows a variation of the *H* component measured using magnetometers at the equatorial station, Jicamarca (blue), and

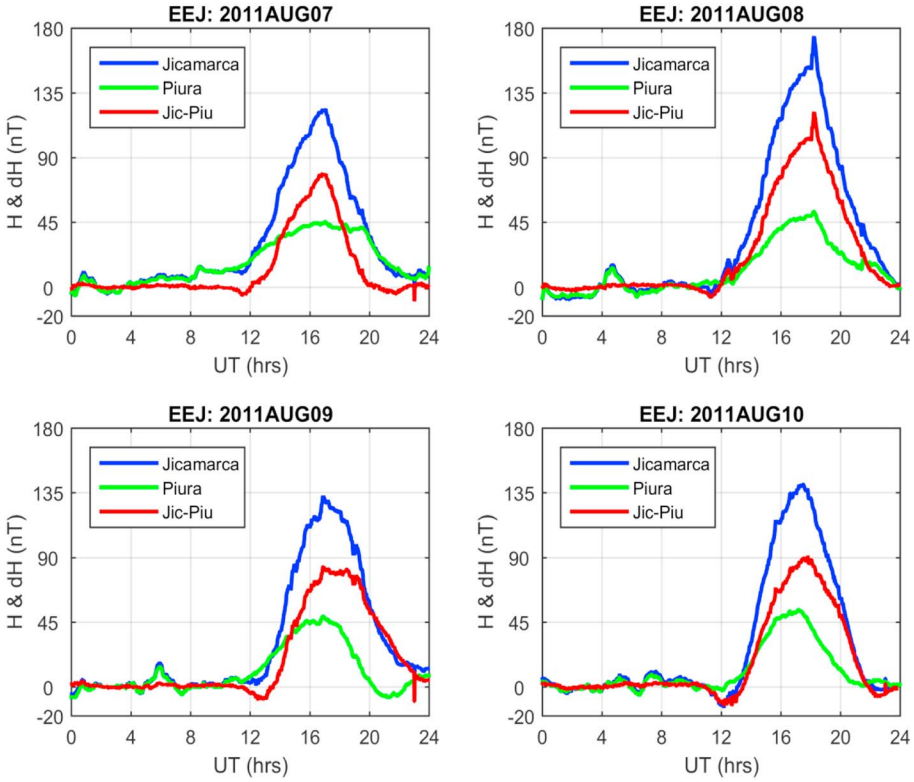

Figure 3. *H* component magnetic field and the difference between two magnetometer stations to show the noontime enhancement of the equatorial electrojet (EEJ) to be used as proxy for the eastward electric field.

off-equatorial station, Piura (green), in the American low latitudes. The red curve represents the net EEJ strength that is enhanced during local noontime.

Figure 4 characterizes ionospheric plasma drifts measured with the Jicamarca ISR on the same days of Figure 3. Data are restricted to the height range of 250 to 400 km for the analysis, thus reducing uncertainties in the measurements caused by increased scatter from higher plasma densities. Not surprisingly, the variations of the ISR drift follow exactly the same patterns of EEJ, with the maximum measured values of the drifts observed at noontime along with the maximum EEJ strengths. By comparing Figure 3 and Figure 4, it is demonstrated that the stronger the EEJ strengths, the faster is the ISR plasma drifts. The diurnal configuration of vertical plasma drift mimics exactly the variation pattern of the electric field supported by EEJ measurements. This correlation between the plasma drift and the EEJ current is quite typical in the equatorial and low-latitude regions since both of these are based on the same EEF.

The TEC distributions of Figure 5 show the variability of the EIA during the days presented in Figures 3 and 4. This figure shows the TEC variation as a function of geomagnetic latitude and universal time (UT). The anomaly crests are intense and have great latitudinal separation if there is strong EEJ leading to a higher value of plasma drifts. The weaker EEJ day has a small drift that is unable to build an effective plasma fountain for the creation of EIAs. Besides equatorial vertical drift, the day-to-day TEC variability in Figure 5 can also be related to changes in solar radiations even though the solar $F_{10.7}$ might not show big differences on those days. The maximum strengths of anomaly crests appear a few hours after the peak value of EEJ and vertical drift. The unequal strength of anomaly crests leads to the asymmetric structure of EIAs. The evidence and controlling factors behind this phenomenon seen in EIA structure will be discussed in detail in the following sections.

3.3. Comparision of Neutral Wind From LLIONS Model and SOFDI Data

To elucidate the role of the meridional component of neutral wind on EIA asymmetry, a physics-based inverse-modeling approach was taken using the LLIONS model. Herein we utilized 1 week of measured neutral wind data in August 2011, as measured from SOFDI, for simultaneous comparison with LLIONS model results. We have presented 4 days of August 2011 neutral wind data in this discussion (Figure 6) for the coincident observation of ISR drift velocity and EEJ as shown in Figures 3 and 4 respectively.

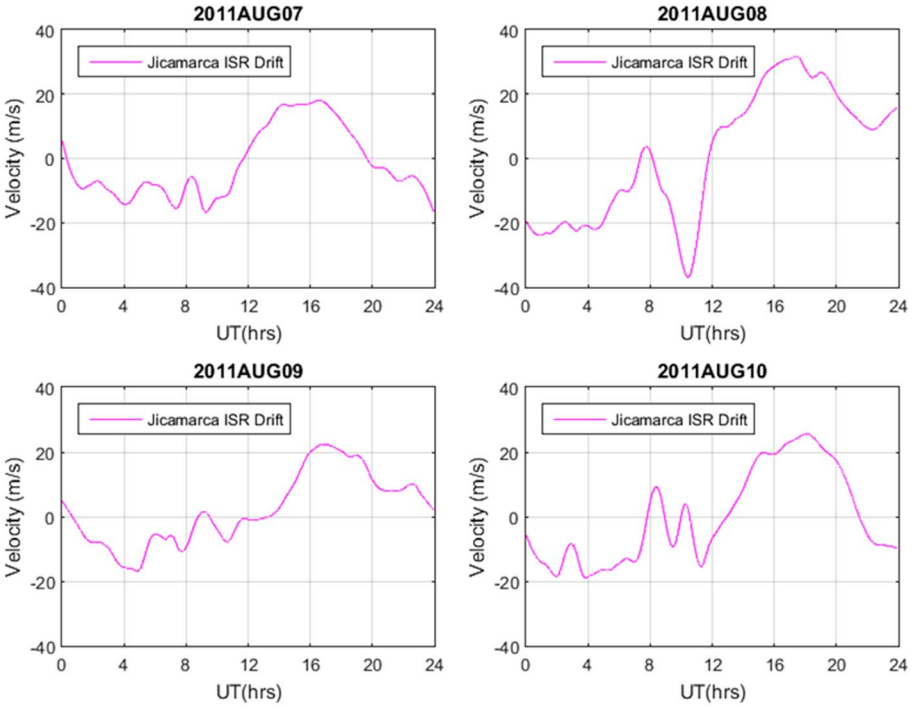

Figure 4. Average vertical plasma drift profiles in the ionosphere from Jicamarca incoherent scatter radar (ISR) at the geomagnetic equator.

The blue curve in Figure 6 displays the meridional neutral wind measured for a whole day at the Huancayo observatory located near the magnetic equator in South America. The green curve in Figure 6 gives the variation of the modeled (LLIONS) meridional neutral wind as a function of Universal time for 4 days (07, 8, 9, and 10 August 2011). The red bars represent the errors of the SOFDI measurements. A very significant day-to-day variability is shown in the SOFDI data. The neutral wind moving northward (southward) direction is called as positive (negative) wind here in the analysis. On 7 August 2011 the wind is positive between 08 and 16 UT and reaches 80 m/s at 12 UT. It is mainly negative during the day. On 8 August 2011, the wind shows values between ±40 m/s except for a period between 00 and 05 UT when it is −40 m/s. The wind value on 9 August 2011 shows a positive peak at 10 UT and mainly negative during the day. On 10 August 2011, the largest

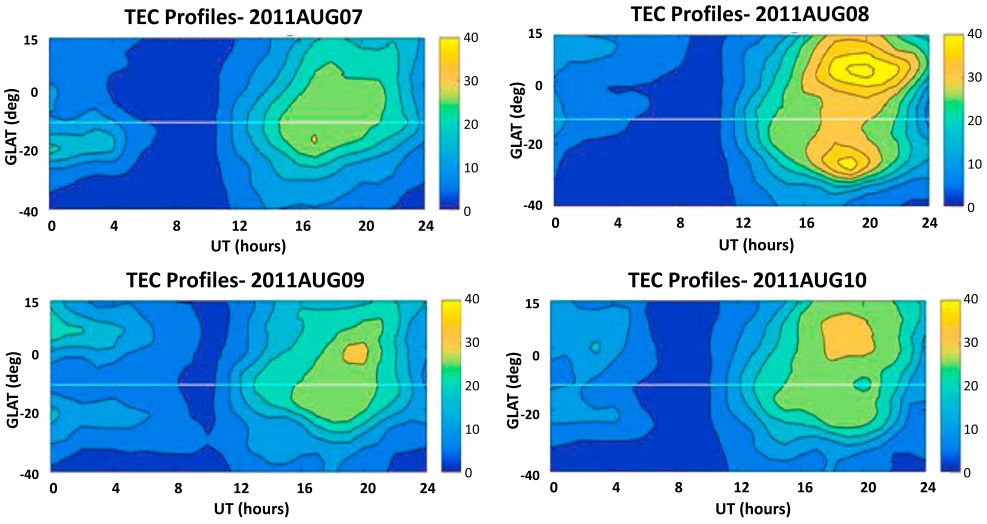

Figure 5. Contour plots of total electron content (TEC) distribution along 70°W on 7, 8, 9, and 10 August 2011. The only figure showing a double-peaked equatorial ionization anomaly is the TEC figure for 8 August 2011. The white horizontal line represents the location of the geomagnetic equatorial line. GLAT, geographic latitude.

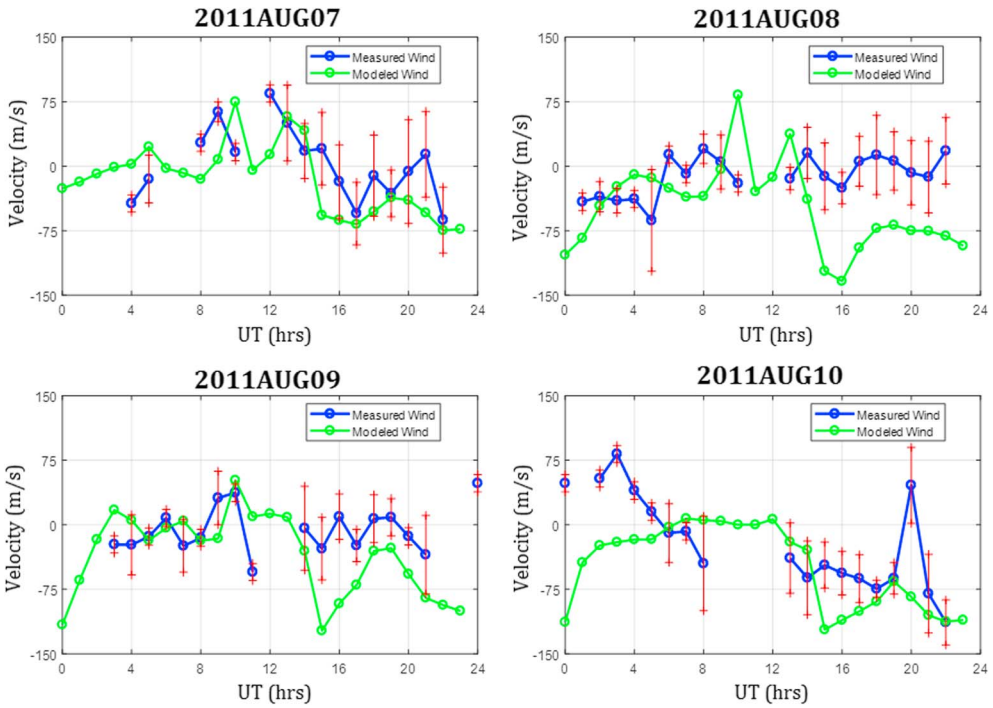

Figure 6. This figure shows the meridional wind velocity for each hour at Huancayo for 7, 8, 9, and 10 August 2011 in the western meridian of American low latitudes. The meridional wind velocities for 8 August 2011 are not large, and this day shows the most symmetric EIA. The blue (green) curve with circles is the measured (modeled) meridional wind velocity by SOFDI (Low-Latitude IONospheric Sector), and the vertical red lines represent the error bars of the measured wind.

temporal fluctuations are shown with the wind varying between +80 m/s at 03 UT and −90 m/s at 22 UT. It is largely negative during the daytime hours.

The LLIONS model, originally inspired by the Anderson (1973) Low-Latitude Ionosphere Model (LOWLAT), is based on the low-latitude portion of the Ionospheric Forecast Model (Schunk et al., 1997). LLIONS calculates the two-dimensional, time-dependent density distributions of five major plasma constituents (NO^+, O_2^+, H^+, O^+, e^-) between ±45° latitude and 90–4,000 km altitude. The plasma distribution is solved along magnetic field lines with many field lines used to construct a regular output 2D grid in magnetic latitude and altitude. Inputs to the model are the vertical $\mathbf{E} \times \mathbf{B}$ drift velocities, horizontal neutral winds, the neutral atmospheric densities and temperatures, and the K_p and $F_{10.7}$ solar flux indices.

An ensemble of 143 independent runs is conducted keeping the vertical drift the same for each of the model runs, but using different meridional winds for each model run. The Horizontal Wind Model (as presented in Hedin et al., 1991) provides both the zonal and the meridional wind values as a function of latitude, longitude, altitude, and universal time W (lat, long, alt, UT). To generate 143 different functions of the wind, we multiplied W (lat, long, alt, UT), as given by the Horizontal Wind Model, by a variable factor (F1) and added another variable factor (F2). The following expression is used to generate the ensemble of wind functions: F1 × W (lat, lon, alt, UT) + F2, where the F1 factor is varied between 0.2 and 2.2 in steps of 0.2 (11 factors) and the F2 additional wind value is increased between −120 and + 120 m/s in steps of 20 m/s (13 numbers). The result of each model run provides a two-dimensional density profile over the 75°W longitude sector. The density profiles are then used to derive TEC latitudinal distributions. Each modeled TEC profile is cross-correlated with the TEC values observed in the Peruvian sector (recall that SOFDI is located at a geographic latitude = −12°). Although this method can introduce, in some extreme cases, unrealistic wind values, it retains the latitudinal and height variability of the meridional wind.

A clear example of the latitudinal variability of the meridional wind values that were obtained with the ensemble model runs is depicted in Figure 7. This figure shows the latitudinal distribution of the wind system that provided the maximum cross-correlation coefficient for 9 August 2011 between 00 and 06. Figure 7 shows the meridional wind to be negative at northern latitudes, then reversing and becoming positive in the Southern Hemisphere. The latitude where the wind reverses varies between 50°S observed at 00 UT

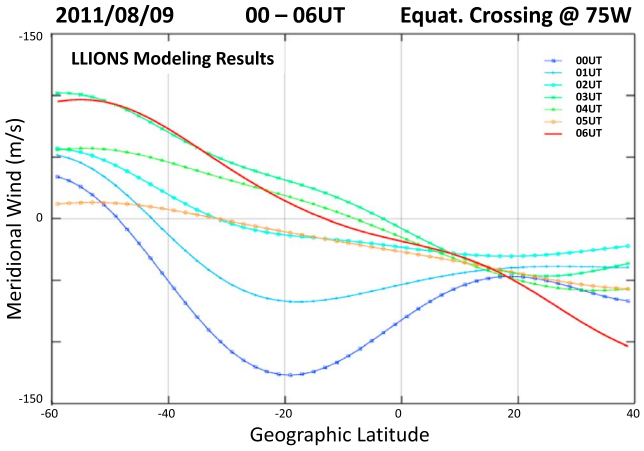

Figure 7. Plot showing a variation of Low-Latitude IONospheric Sector (LLIONS)-modeled meridional neutral wind against geographic latitude for 7 hr.

and −12°S (near the magnetic equator) at 06 UT. It is worth mentioning that the meridional wind of 00 UT (Figure 7) produced one of the largest values (−110 m/s) at the magnetic equator (see Figure 6).

A close comparison between the meridional neutral wind estimated from the ensemble of LLIONS runs and SOFDI measurements shows a reasonable agreement with respect to magnitude and direction. During quiet days, electric field fluctuations in the EEJ altitudes are rare because the background electric field mostly overwhelms wind-driven perturbation electric fields (Kelley, 2009; Shume et al., 2014). The modeled patterns of meridional neutral wind also show a trend similar to the variations of the SOFDI measurements. The best agreement was obtained on 7 August 2011 when the derived winds are between the error bars of the measured wind. On 8 an d 9 August 2011, the calculated winds approximate the SOFDI measured winds between 04 and 14 UT. In general, one can see that the meridional neutral wind derived by the inverse modeling shows a good qualitative agreement rather than quantitative with the measured values presented in Figure 6. This result indicates that further improvements of the inverse model procedure are needed to get a quantitative agreement with the measured wind. It is suggested to consider the altitude dependence of the vertical drifts that is measured with the Jicamarca radar and can be used as input to the LLIONS model.

A comparison of the TEC contours of Figure 5 and the meridional winds of Figure 6 points out the close relationship of the meridional wind and the EIA asymmetry. On 7, 9, and 10 August, the meridional wind is negative between 16 and 24 UT when the EIA shows an asymmetry with a pronounced northern crest. On 8 August 2011, the SOFDI winds show small fluctuations around zero making the anomaly more symmetric.

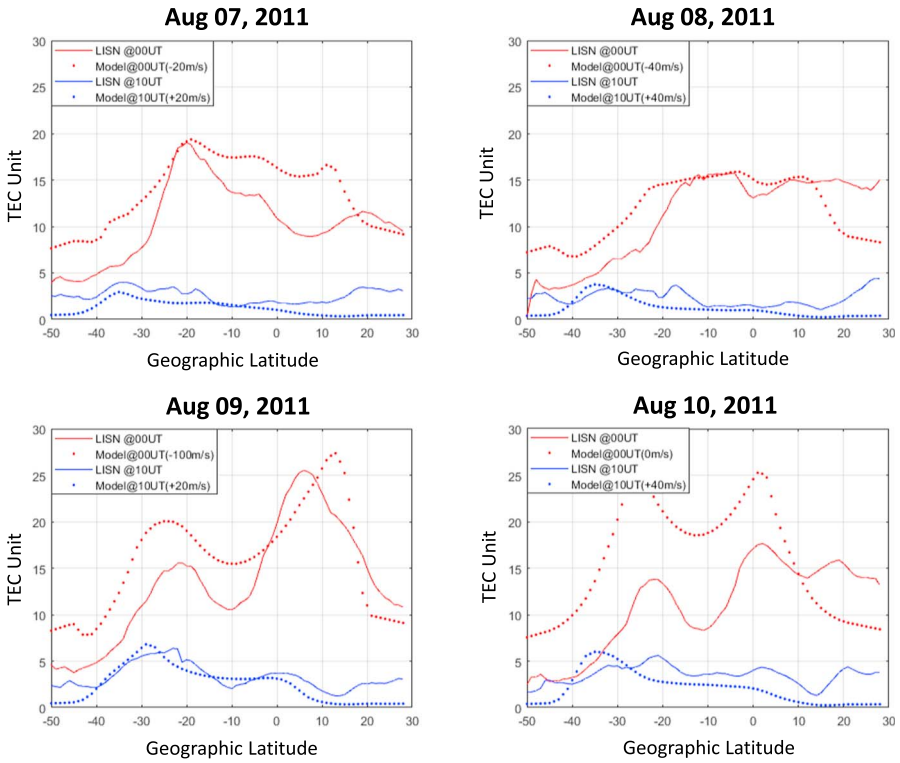

Figure 8. Plots showing a comparison of Low-Latitude Ionospheric Sensor Network (LISN)-measured (continuous curves) and Low-Latitude IONospheric Sector (LLIONS)-modeled (dotted curves) total electron content (TEC) variations against geographic latitude. In each panel, TEC values are binned in every degree of latitude and plot its variation at 00 UT (red) and 10 UT (blue) for both measured and modeled cases.

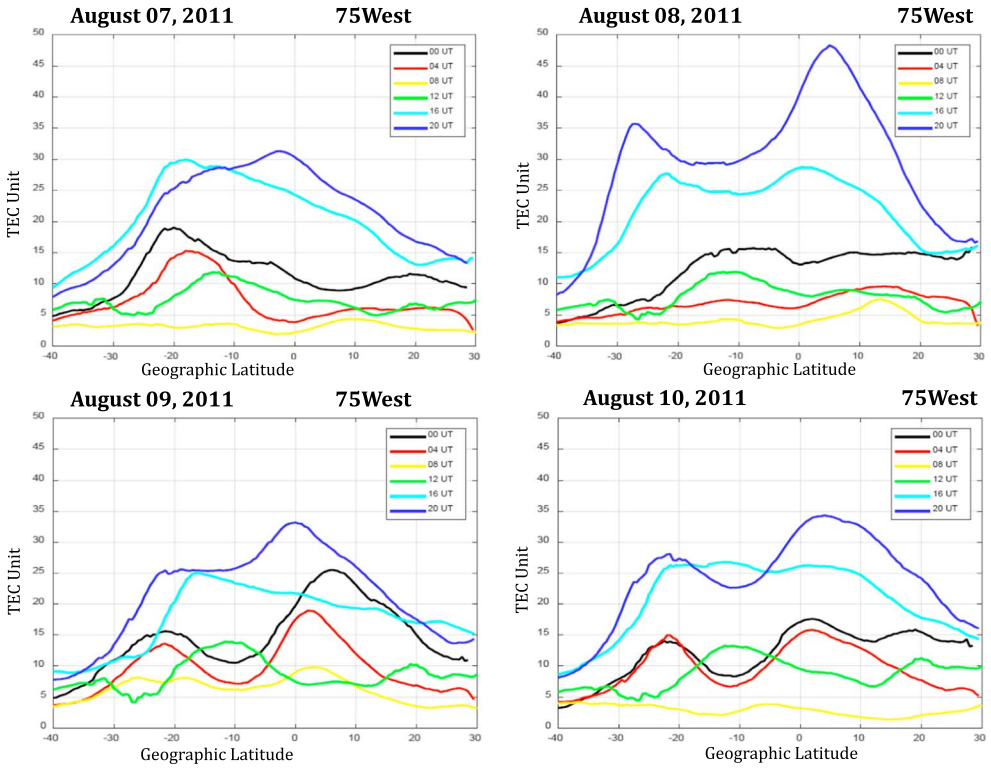

Figure 9. Latitudinal profiles of total electron content (TEC) in the 4-hr interval against geographic latitude for 7, 8, 9, and 10 August 2011 in the western meridian of South America.

Figure 8 presents the comparison of measured TEC and modeled (LLIONS) TEC values. The latter were calculated using neutral winds estimated using the inverse modeling approach. The general trends and magnitudes of TEC from GPS and model values look comparable in most of the cases. In Figure 8, it is seen that model TEC values follow exactly the same magnitude and pattern as LISN measurement at 10 UT. However, there are some discrepancies between measured and model TEC at 00 UT. For example, in Figure 8, the model and measured peak values of TEC on 7 and 8 August 2011 are highly correlated with each other regarding their magnitudes as well as in trends. While on 9 and 10 August 2011, the magnitudes of TEC values are poorly correlated, but their trends are similar. In Figure 8, as the meridional neutral wind is positive (northward), the southern anomaly peaks in terms of TEC seem to shift farther from the equator towards the Southern Hemisphere. These cases are seen in all the subplots of Figure 8 at 10 UT. For the conditions of negative (southward) meridional neutral wind, the southern anomaly peaks seem to come closer toward the equator from the Southern Hemisphere. It is to be noted that the actual measured Jicamarca ISR vertical drift is one of the inputs in the model discussed here. However, the model does not consider the zonal ion drifts, neutral winds other than meridional, and variations of the O/N_2 ratio. These might be some of the sources of discrepancies in our results. Furthermore, the results presented here are for only 4 days of August of 2011. The 24-hr measured neutral wind data cannot give a detailed picture for the inference but gives the sense of interpretation of meridional neutral wind patterns for the EIA anomalies.

Figure 9 shows TEC latitudinal profiles measured by several networks of GPS receivers in the Peruvian sector (~75°W). These plots are used to relate the asymmetry of the anomaly to the sign of the meridional wind that was measured by SOFDI. The TEC anomaly curves show symmetric characteristics on 8 August 2011 between 08 and 16 UT (magnetic equator = 12°S). A highly asymmetric anomaly containing a predominant southern crest was observed on 7 August 2011, between 12 and 16 UT. An asymmetric anomaly with a dominant northern crest was measured on all 4 days at 20 UT. These symmetric and asymmetric characteristics of the anomaly are related to meridional wind. For example, on 8 August 2011, the SOFDI winds fluctuate around 0 m/s and do not influence the development of any crests. On 7 August and between 12 and 16, the meridional wind has been positive for more than 4 hr, making the plasma to move up the field lines in the Southern Hemisphere and down in the Northern Hemisphere. The same effect is seen in the wind

value near 20 UT for each of the plots. The velocity is negative or follows a long period of negative velocities that enables the development of a northern crest.

4. Interpretation and Discussion

Trans-equatorial neutral winds can have profound influences on numerous ionospheric processes including plasma transport, composition, and the formation of structured EIAs. We have demonstrated the contribution of the EEJ and meridional neutral wind on the prevailing asymmetry structure in EIA in the low-latitude ionosphere using measured as well as model data. In general, the strength, latitudinal extension, and symmetry/asymmetry of the anomaly crests are based on regular equatorial ionospheric electrodynamical phenomena (e.g., both zonal electric field and meridional wind). It is evidently speculated that in the absence of external perturbations, the EEJ associated with zonal electric field can alone form the symmetric structure of EIAs in the low-latitude ionosphere. Observations and model results show the significant role of the meridional neutral wind that blows the ionospheric plasma toward the opposite hemisphere by moving the plasma along geomagnetic field lines to generate the asymmetric structure characteristics of the equatorial anomaly (Bailey et al., 1973; Schunk & Nagy, 2000; Venkatraman & Heelis, 2000).

The motion of ionized particles at ionospheric heights is affected by the Earth's magnetic field, which in turn controls the flow of the ionospheric currents as well as the bulk movement of the plasma. The EEF and the particular geometry of the geomagnetic field lift the plasma to higher altitudes over the equator. As the vertical drift of plasma is canceled by the gravitational and pressure forces, the plasma starts moving along the flux tube of the Earth's magnetic field that transports plasma to poleward latitudes from the equator, forming the EIA. The occurrence of daytime maximum EEJ and well-developed EIA varies in the time range difference of 2.5 to 5 hr over the low-latitude sectors (Abdu et al., 1990; Venkatesh et al., 2015). Our analysis also lies within the already reported time frame for those parameters.

The EIA occurs during the major part of the day, and its intense ionization density irregularities distinguish the low-latitude ionosphere from other regions. Its asymmetry structure can be explained in terms of neutral wind. The winds transport particle mass, momentum, and energy throughout the atmosphere. The wind also moves plasma through drag/collisions and can induce currents and electric fields. Waves also propagate within the neutral atmosphere and can perturb the normal behavior of the thermosphere. Once gravity waves and tides reach the ionospheric height, due to the neutral-ions collision of the closely coupled ions and neutrals, momentum from neutrals is transferred to ions. The ultimate fate of this phenomenon is the formation of asymmetry of ionospheric plasma concentration in EIAs. Figures 5, 6, and 9 have shown that when the meridional wind is near zero, a symmetric anomaly is observed. Figure 9 indicated that a positive (south to north) wind is associated with a dominant southern crest, and for negative meridional wind, a northern crest prevails. These relationship supports intra-hemisphere transport of plasma in the anomaly region.

The population and distribution of excited neutral and/ or ionized species in different ionospheric regions depend not only on chemical processes (production, collision, and recombination) but also on transport processes associated with field domains and neutral winds (Schunk & Nagy, 2000). One of the key points of this study was to characterize the performance of the models over measured neutral wind for the understanding of EIA asymmetry. Further measurements are clearly needed with higher resolution and corresponding sensitivities to the daytime wind occurrences of interest for the detailed explanation of TEC asymmetry in EIAs. It is known that there are various factors that can cause EIA asymmetry in the low-latitude ionosphere. The role of meridional neutral winds on EIA asymmetry generation can be explained in the following ways:

1. Intra-hemisphere Transport: The neutral winds system has the ability to move the ions and electrons along the geomagnetic field lines and affects its densities because of the height-dependent nature of the plasma chemical recombination in the *F* region ionosphere (Hargreaves, 1992; Sastri, 1990). If the meridional neutral wind is blowing north to south (south to north), it will drive plasma to higher ionospheric heights along field lines where recombination proceeds at a slower pace. This leads to higher plasma density in the Northern (Southern) Hemisphere. Then the population of ionospheric plasma is enhanced since a strong equatorial plasma fountain restricts the effect of wind in windward locations over that in leeward locations. Figure 10a illustrates this case scenario where plasma density increases in the Northern Hemisphere.

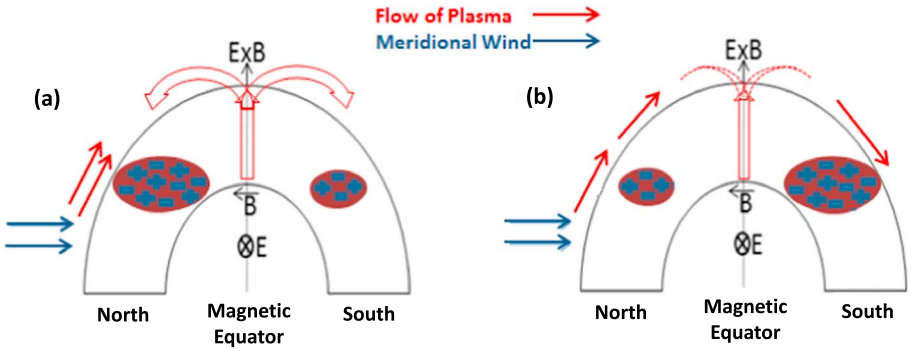

Figure 10. A cartoon illustration showing possible evolution and mechanism how meridional neutral wind creates asymmetry in equatorial ionization (EIA) anomaly in the ionospheric *F* layer, looking eastward (a) intra-hemisphere transport and (b) trans-equatorial transport. The size of the shaded oval shape represents the strength of the EIA crest in the two hemispheres.

2. Trans-equatorial Transport: The interhemispheric field-aligned plasma flow organized by season and longitude, depending on the role of meridional wind, can be seen during the time of adiabatic heating and cooling at ionospheric heights (Bailey et al., 1973; Venkatraman & Heelis, 2000). If the meridional neutral wind is blowing north to south (south to north), it will transport plasma along the Earth's magnetic field lines and will dump at ionospheric height in the opposite hemisphere since the effect of a weak equatorial plasma fountain is easily overcome by wind. That leads to a higher plasma density in the Southern (Northern) Hemisphere than that in northern (southern) crests. Then the population of ionospheric plasma is less in the windward location than leeward location. Figure 10b illustrates this case scenario where ions have the time to be transported to the opposite hemisphere and form asymmetry in EIAs.

Based on observation and modeling, the mechanism described in the first method explains most of the asymmetry events of the EIA.

5. Summary and Conclusions

This study compares 24-hr measured and modeled meridional neutral winds and investigates in detail its effects on the asymmetry of the EIA. The analysis leads to a significant advance in the study of the EIA and opens new avenues for future studies into the climatology and relationships of the EEF, EEJ, neutral winds, and EIA, during both quiet and active solar/geomagnetic conditions. The major outcomes from our study are outlined as follows:

1. The vertical $\mathbf{E} \times \mathbf{B}$ plasma drift associated with EEF and geomagnetic fields, as well as the neutral wind fields, are the main drivers of EIA anomaly. The meridional component of the thermospheric wind is one of the most significant drivers of the EIA asymmetry. The neutral particles use collision to transport ions up the field, but the plasma remains within the same hemisphere.
2. The northward (southward) propagation of intense TEC crest is clearly visible in the northern (southern) hemispheric summer seasons, while northward (southward) TEC crests during equinox periods remained intact at almost similar latitudinal locations. The latitudinal distribution of asymmetry in the intensity of northward and southward spread is caused by the different motion caused by a wind dynamo. The latitudinal extension and strength of anomaly crests are controlled by EEF that is seen as a proxy of the EEJ development, but meridional neutral wind mainly acted to create unequal strengths of the crests to form anomaly asymmetries in the low latitudes.
3. The meridional neutral wind profiles, which also play a decisive role for the generation of asymmetry structure in the EIA, can be estimated using the LLIONS model, which utilizes vertical drift measured from Jicamarca ISR as one of the inputs. It shows reasonably good agreement within the error range of measurements by SOFDI at the geomagnetic equator for similar conditions, which strengthens the confidence of our results.
4. The anomaly crests look more symmetric in equinox than in solstice seasons. The asymmetries of the EIA observed during December solstice is greater than during June solstice, whereas September equinox is less symmetric than March equinox seasons. This variability is related to the seasonal dependence of the vertical drift (Fejer, 1991) and meridional wind.

This effect of meridional neutral wind on the EIA asymmetry is a key mechanism for the vertical and latitudinal coupling between different atmospheric layers and also provides an important input on various forms of atmospheric mechanisms such as tides, density fluctuation, drift variability, wind dynamo, and even the extension of the EIA from low to middle latitudes. Further analysis and investigation with real-time data are continuing for a better understanding of the meridional wind including zonal wind patterns on thermosphere/neutral composition and the ionosphere over the magnetic equator and the response of EIA under quiet and magnetosphere-induced disturbed conditions.

Acknowledgments
We would like to thank Director Patricia H. Doherty and Research Scientist Rezy Pradipta of the Institute for Scientific Research, Boston College, for their helpful comments and suggestions on the paper. One of the authors, C. E. Valladares, was partially supported by National Science Foundation (NSF) grants AGS-1552161, AGS-1563025, and AGS-1724133. He was also supported by Office of Naval Research contract N-00014-17-1-2157. Moreover, A. J. Gerrard acknowledges the support of the Geophysical Institute of Peru in maintaining the SOFDI instrument. The LISN is a project led by The University of Texas at Dallas in collaboration with the Geophysical Institute of Peru and other institutions that provide information in benefit of the scientific community. We thank all organizations and persons that are supporting and operating receivers in LISN. The TEC values presented in this publication are stored in the LISN Web page (http://lisn.igp.gob.pe).

References

Abdu, M. A., Brum, C. G. M., Batista, I. S., Sobral, J. H. A., de Paula, E. R., & Souza, J. R. (2008). Solar flux effects on equatorial ionization anomaly and total electron content over Brazil: Observational results versus IRI representations. *Advances in Space Research*, *42*(4), 617–625. https://doi.org/10.1016/j.asr.2007.09.043

Abdu, M. A., Walker, G. O., Reddy, B. M., Sobral, J. H. A., Fejer, B. G., Kikuchi, T., et al. (1990). Electric field versus neutral wind control of the equatorial anomaly under quiet and disturbed condition: A global perspective from SUNDIAL 86. *Annales Geophysique*, *8*, 419–430.

Anderson, D. N. (1973). A theoretical study of the ionospheric *F* region equatorial anomaly, I, theory. *Planetary and Space Science*, *21*(3), 409–419. https://doi.org/10.1016/0032-0633(73)90040-8

Appleton, E. V. (1946). Two anomalies in the ionosphere. *Nature*, *157*(3995), 691. https://doi.org/10.1038/157691a0

Bailey, G. J., Moffett, R. J., Hanson, W. B., & Sanatani, S. (1973). Effects of interhemisphere transport on plasma temperatures at low latitudes. *Journal of Geophysical Research*, *78*(25), 5597–5610. https://doi.org/10.1029/JA078i025p05597

Balan, N., Bailey, J. J., Moffett, R. J., Su, Y. Z., & Titheridge, J. E. (1995). Modeling studies of the conjugate-hemisphere differences in ionospheric ionization at equatorial anomaly latitudes. *Journal of Atmospheric and Terrestrial Physics*, *57*(3), 279–292. https://doi.org/10.1016/0021-9169(94)E0019-J

Baumjohann, W., & Treumann, R. A. (2012). *Basic space plasma physics* (Revised ed.). London: Imperial College Press. https://doi.org/10.1142/p850

Blanc, M., & Richmond, A. D. (1980). The ionospheric disturbance dynamo. *Journal of Geophysical Research*, *85*(A4), 1669–1686. https://doi.org/10.1029/JA085iA04p01669

Burnside, R. G., Herrero, F. A., Meriwether, J. W., & Walker, J. C. G. (1981). Optical observations of thermospheric dynamics at Arecibo. *Journal of Geophysical Research*, *86*(A7), 5532–5540. https://doi.org/10.1029/JA086iA07p05532

Chapman, S. (1951). The equatorial electrojet as detected from the abnormal electric current distribution above Huancayo, Peru and elsewhere. *Archiv für Meteorologie, Geophysik und Bioklimatologie Serie A*, *4*(1), 368–390. https://doi.org/10.1007/BF02246814

Dang, T., Luan, X., Lei, J., Dou, X., & Wan, W. (2016). A numerical study of the interhemispheric asymmetry of the equatorial ionization anomaly in solstice at solar minimum. *Journal of Geophysical Research: Space Physics*, *121*, 9099–9110. https://doi.org/10.1002/2016JA023012

Deshpande, M. R., Rastogi, R. G., Vats, H. O., Klobuchar, J. A., Sethia, G., Jain, A. R., et al. (1977). Effect of electrojet on the total electron content of the ionosphere over the Indian subcontinent. *Nature*, *267*(5612), 599–600. https://doi.org/10.1038/267599a0

Dunford, E. (1967). The relationship between the ionospheric equatorial anomaly and the *E*-region current system. *Journal of Atmospheric and Terrestrial Physics*, *29*(12), 1489–1498. https://doi.org/10.1016/0021-9169(67)90102-X

Eccles, V., Rice, D. D., Sojka, J. J., Valladares, C. E., Bullett, T., & Chau, J. L. (2011). Lunar atmospheric tidal effects in the plasma drifts observed by the Low-Latitude Ionospheric Sensor Network. *Journal of Geophysical Research*, *116*, A07309. https://doi.org/10.1029/2010JA016282

Egedal, J. (1947). The magnetic diurnal variation of the horizontal force near magnetic equator. *Journal of Geophysical Research*, *52*(4), 449–451. https://doi.org/10.1029/TE052i004p00449

Fejer, B. G. (1991). Low latitude electrodynamic plasma drifts: A review. *Journal of Atmospheric and Terrestrial Physics*, *53*(8), 677–693. https://doi.org/10.1016/0021-9169(91)90121-M

Forbes, J. M. (1981). The equatorial electrojet. *Reviews of Geophysics*, *19*(3), 469–504. https://doi.org/10.1029/RG019i003p00469

Gerrard, A. J., & Meriwether, J. W. (2011). Initial daytime and nighttime SOFDI observations of thermospheric winds from Fabry-Perot Doppler shift measurements of the 630-nm OI line-shape profile. *Annales Geophysique*, *29*(9), 1529–1536. https://doi.org/10.5194/angeo-29-1529-2011

Goncharenko, L. P., Coster, A. J., Chau, J. L., & Valladares, C. E. (2010). Impact of sudden stratospheric warmings on equatorial ionization anomaly. *Journal of Geophysical Research*, *115*, A00G07. https://doi.org/10.1029/2010JA015400

Hanson, W. B., & Moffett, R. J. (1966). Ionization transport effects in the equatorial *F* region. *Journal of Geophysical Research*, *71*(23), 5559–5572 . https://doi.org/10.1029/JZ071i023p05559

Hargreaves, J. K. (1992). *The solar-terrestrial environment*. Cambridge, UK: Cambridge University Press. https://doi.org/10.1017/CBO9780511628924

Hedin, A. E., Biondi, M. A., Burnside, R. G., Hernandez, G., Johnson, R. M., Killeen, T. L., et al. (1991). Revised global model of thermosphere winds using satellite and ground-based observations. *Journal of Geophysical Research*, *96*(A5), 7657–7688. https://doi.org/10.1029/91JA00251

Heelis, R. A. (2004). Electrodynamics in the low and middle latitude ionosphere: A tutorial. *Journal of Atmospheric and Solar-Terrestrial Physics*, *66*(10), 825–838. https://doi.org/10.1016/j.jastp.2004.01.034

Hei, M. A., & Valladares, C. E. (2010). The November 2004 superstorm: Comparison of low latitude TEC observations with LLIONS model results. *Journal of Atmospheric and Solar-Terrestrial Physics*, *72*(4), 334–343. https://doi.org/10.1016/j.jastp.2009.03.025

Immel, T. J., Sagawa, E., England, S. L., Henderson, S. B., Hagan, M. E., Mende, S. B., et al. (2006). Control of equatorial ionospheric morphology by atmospheric tides. *Geophysical Research Letters*, *33*, L15108. https://doi.org/10.1029/2006GL026161

Jonah, O. F., de Paula, E. R., Muella, M. T. A. H., Dutra, S. L. G., Kherani, E. A., Negreti, P. M. S., & Otsuka, Y. (2015). TEC variation during high and low solar activities over South American sector. *Journal of Atmospheric and Solar-Terrestrial Physics*, *135*, 22–35. https://doi.org/10.1016/j.jastp.2015.10.005

Kelley, M. C. (2009). *The Earth's ionosphere: Plasma physics and electrodynamics* (2nd ed.). Cambridge, MA: Academic Press.

Khadka, S. M., Valladares, C., Pradipta, R., Pacheco, E., & Condor, P. (2016). On the mutual relationship of the equatorial electrojet, TEC and scintillation in the Peruvian sector. *Radio Science*, *51*, 742–751. https://doi.org/10.1002/2016RS005966

Laundal, K. M., Cnossen, I., Milan, S. E., Haaland, S. E., Coxon, J., Pedatella, N. M., et al. (2016). North–south asymmetries in Earth's magnetic field. *Space Science Reviews*, *206*(1-4), 225–257. https://doi.org/10.1007/s11214-016-0273-0

Lin, C. H., Richmond, A. D., Bailey, G. J., Liu, J. Y., Lu, G., & Heelis, R. A. (2009). Neutral wind effect in producing a storm time ionospheric additional layer in the equatorial ionization anomaly region. *Journal of Geophysical Research*, *114*, A09306. https://doi.org/10.1029/2009JA014050

Luan, X., Wang, P., Dou, X., & Liu, Y. C.-M. (2015). Interhemispheric asymmetry of the equatorial ionization anomaly in solstices observed by COSMIC during 2007–2012. *Journal of Geophysical Research: Space Physics*, *120*, 3059–3073. https://doi.org/10.1002/2014JA020820

MacDougall, J. W. (1969). The equatorial ionospheric anomaly and equatorial electrojet. *Radio Science*, *4*(9), 805–810. https://doi.org/10.1029/RS004i009p00805

Makela, J. J., Fisher, D. J., Meriwether, J. W., Buriti, R. A., & Medeiros, A. F. (2013). Near-continual ground-based nighttime observations of thermospheric neutral winds and temperatures over equatorial Brazil from 2009 to 2012. *Journal of Atmospheric and Solar - Terrestrial Physics*, *103*, 94–102. https://doi.org/10.1016/j.jastp.2012.11.019

Makela, J. J., Meriwether, J. W., Ridley, A. J., Ciocca, M., & Castellez, M. W. (2012). Large-scale measurements of thermospheric dynamics with a multisite Fabry-Perot interferometer network: Overview of plans and results from midlatitude measurements. *International Journal of Geophysics*, *2012*, 1–10. https://doi.org/10.1155/2012/872140

Martyn, D. F. (1947). Atmospheric tides in the ionosphere. 1. Solar tides in the F_2 region. *Proceedings of the Royal Society of London A*, *189*(1017), 241–260. https://doi.org/10.1098/rspa.1947.0037

Meriwether, J. W. (2006). Studies of thermospheric dynamics with a Fabry-Perot interferometer network: A review. *Journal of Atmospheric and Solar-Terrestrial Physics*, *68*(13), 1576–1589. https://doi.org/10.1016/j.jastp.2005.11.014

Onwumechili, C. A. (1997). *The equatorial electrojet*. Amsterdam, The Netherlands: Gordon and Breach Science Publishers.

Richmond, A. D. (1989). Modeling the ionospheric wind dynamo: A review. *Pure and Applied Geophysics*, *131*(3), 413–435. https://doi.org/10.1007/BF00876837

Rishbeth, H. (1972). Thermospheric winds and the *F*-region: A review. *Journal of Atmospheric and Terrestrial Physics*, *34*(1), 1–47. https://doi.org/10.1016/0021-9169(72)90003-7

Rishbeth, H. (1997). The ionospheric *E*-layer and *F*-layer dynamos—A tutorial review. *Journal of Atmospheric and Space Physics*, *59*(15), 1873–1880. https://doi.org/10.1016/S1364-6826(97)00005-9

Sastri, J. H. (1990). Equatorial anomaly in *F* region: A review. *Indian Journal of Radio & Space Physics*, *19*, 225–240.

Schunk, R. W., & Nagy, A. F. (2000). *Ionosphere: Physics, plasma and chemistry*. New York: Cambridge University Press. https://doi.org/10.1017/CBO9780511551772

Schunk, R. W., Sojka, J. J., & Eccles, J. V. (1997). Expanded capabilities for the ionospheric forecast model, Rep. AFRL-VS-HA-TR-98-0001, Space Vehicles Dir., Air Force Res. Lab., Hanscom AFB, Bedford, MA.

Shume, E. B., Rodrigues, F. S., Mannucci, A. J., & de Paula, E. R. (2014). Modulation of equatorial electrojet irregularities by atmospheric gravity waves. *Journal of Geophysical Research: Space Physics*, *119*, 366–374. https://doi.org/10.1002/2013JA019300

Sojka, J., Raitt, W., & Schunk, R. (1979). Effect of displaced geomagnetic and geographic poles on high-latitude plasma convection and ionospheric depletions. *Journal of Geophysical Research*, *84*(A10), 5943–5951. https://doi.org/10.1029/JA084iA10p05943

Stolle, C., Manoj, C., Lühr, H., Maus, S., & Alken, P. (2008). Estimating the daytime equatorial ionization anomaly strength from electric field proxies. *Journal of Geophysical Research*, *113*, A09310. https://doi.org/10.1029/2007JA012781

Su, Y. Z., Bailey, G. J., Oyama, K. I., & Balan, N. (1997). A modelling study of the longitudinal variations in the north-south asymmetries of the ionospheric equatorial anomaly. *Journal of Atmospheric and Terrestrial Physics*, *59*(11), 1299–1310. https://doi.org/10.1016/S1364-6826(96)00016-8

Titheridge, J. E. (1995). Winds in the ionosphere—Review. *Journal of Atmospheric and Terrestrial Physics*, *57*(14), 1681–1714. https://doi.org/10.1016/0021-9169(95)00091-F

Tulasi Ram, S., Su, S. Y., & Liu, C. H. (2009). FORMOSAT-3/COSMIC observations of seasonal and longitudinal variations of equatorial ionization anomaly and its interhemispheric asymmetry during the solar minimum period. *Journal of Geophysical Research*, *114*, A06311. https://doi.org/10.1029/2008JA013880

Valladares, C. E., & Chau, J. L. (2012). The Low-Latitude Ionospheric Sensor Network: Initial results. *Radio Science*, *47*, RS0L17. https://doi.org/10.1029/2011RS004978

Venkatesh, K., Fagundes, P. R., Prasad, D. S. V. V. D., Denardini, C. M., de Abreu, A. J., de Jesus, R., & Gende, M. (2015). Day-to-day variability of equatorial electrojet and its role on the day-to-day characteristics of the equatorial ionization anomaly over the Indian and Brazilian sectors. *Journal of Geophysical Research: Space Physics*, *120*, 9117–9131. https://doi.org/10.1002/2015JA021307

Venkatraman, S., & Heelis, R. (2000). Interhemispheric plasma flows in the equatorial topside ionosphere. *Journal of Geophysical Research*, *105*(A8), 18,457–18,464. https://doi.org/10.1029/2000JA000012

Xiong, C., Lühr, H., & Ma, S. Y. (2013). The magnitude and inter-hemispheric asymmetry of equatorial ionization anomaly-based on CHAMP and GRACE observations. *Journal of Atmospheric and Terrestrial Physics*, *105-106*, 160–169. https://doi.org/10.1016/j.jastp.2013.09.010